
Multi-way Encoding for Robustness

Donghyun Kim
Boston University

Sarah Adel Bargal
Boston University

Jianming Zhang
Adobe Research

Stan Sclaroff
Boston University

Abstract

Deep models are state-of-the-art for many computer vision tasks including image classification and object detection. However, it has been shown that deep models are vulnerable to adversarial examples. We highlight how one-hot encoding directly contributes to this vulnerability and propose breaking away from this widely-used, but highly-vulnerable mapping. We demonstrate that by leveraging a different output encoding, multi-way encoding, we decorrelate source and target models, making target models more secure. Our approach makes it more difficult for adversaries to find useful gradients for generating adversarial attacks of the target model. We present robustness for black-box and white-box attacks on four benchmark datasets. The strength of our approach is also presented in the form of an attack for model watermarking by decorrelating a target model from a source model.

1 Introduction

Deep learning models are vulnerable to adversarial examples [1]. Evidence shows that adversarial examples are transferable [2, 3]. This weakness can be exploited even if the adversary does not know the target model under attack, posing severe concerns about the security of the models. This is because an adversary can use a substitute model for generating adversarial examples for the target model, also known as *black-box* attacks.

Black-box attacks such as gradient-based attacks [4, 5] rely on perturbing input by adding an amount dependent upon the gradient of the loss function with respect to the input (input gradient) of a substitute model. An example adversarial attack is $x^{adv} = x + \epsilon \text{sign}(\nabla_x \text{Loss}(f(x)))$, where $f(x)$ is the model used to generate the attack. This added “noise” can fool a model although it may not be visually evident to a human. The assumption of such gradient-based approaches is that the gradients with respect to the input, of the substitute and target models, are correlated.

Our key observation is that the setup of conventional deep classification frameworks aids in the correlation of such gradients, and thereby makes these models more susceptible to black-box-attacks. Typically, a cross-entropy loss, a soft-max layer, and a one-hot vector encoding for a target label are used when training deep models. These conventions constrain the encoding length and the number of possible non-zero gradient directions at the encoding layer. This makes it easier for an adversary to pick a harmful gradient direction and perform an attack from a substitute model.

We aim to increase the adversarial robustness of deep models through *model decorrelation*. Our multi-way encoding representation relaxes the one-hot encoding to a real number encoding, and embeds the encoding in a space that has a dimension that is higher than the number of classes. These encoding methods lead to an increased number of possible gradient directions, as illustrated in Fig. 1. This makes it more difficult for an adversary to pick a harmful direction that would cause a misclassification. Multi-way encoding also helps improve a model’s robustness in cases where the adversary has full knowledge of the target model under attack: a *white-box* attack. The benefits of multi-way encoding are demonstrated in experiments with four benchmark datasets.

We also demonstrate the strength of *model decorrelation* by introducing an attack for the recent model watermarking algorithm of Zhang *et al.* [6], which deliberately trains a model to misclassify certain

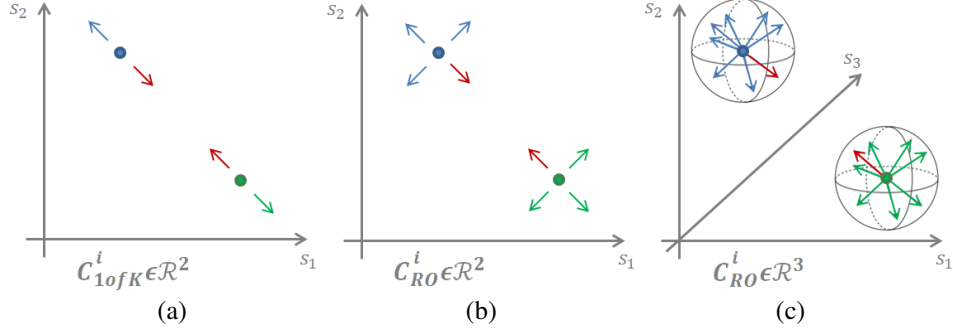


Figure 1: Demonstration of the benefit of relaxing and increasing the encoding dimensionality, for a binary classification problem at the final encoding layer. C_i is the codebook encoding for class i , axis s_i represents the output activation of neuron i in the output encoding layer, where $i = 1, \dots, l$ and l is the encoding dimensionality. The depicted points are correctly classified points of the green and blue classes. The arrows depict the possible non-zero perturbation directions $\text{sign}(\frac{\partial \text{Loss}}{\partial s_i})$. (a) *2D 1ofK softmax-crossentropy setup*: Only two non-zero gradient directions exist for a *1ofK* encoding. Of these two directions, only one is an adversarial direction, depicted in red. (b) *2D multi-way encoding*: Four non-zero perturbation directions exist. The fraction of directions that now move a point to the adversarial class (red) drops. (c) *3D multi-way encoding*: A higher dimensional encoding results in a significantly lower fraction of gradient perturbations whose direction would move an input from the green ground-truth class to the blue class, or vice versa.

watermarked images. We interpret such watermarked images as transferable adversarial examples. We demonstrate that the multi-way encoding reduces the transferability of the watermarked images.

We summarize our contributions as follows:

1. We propose a novel solution using multi-way encoding to alleviate the vulnerability caused by the *1ofK* mapping through *model decorrelation*.
2. We empirically show that the proposed approach improves model robustness against both black-box attacks, white-box attacks, and general corruptions.
3. We also show the strength of our encoding framework by attacking a recently proposed model watermarking algorithm.

2 Related Work

Attacks. Adversarial examples are crafted images for fooling a classifier with small perturbations. Recently, many different types of attacks have been proposed to craft adversarial examples. We focus on gradient-based attacks which deploy the gradient of the loss with respect to the input [4, 7, 8]. Goodfellow *et al.* [4] propose the Fast Gradient Sign Method (FGSM) which generates adversarial images by adding the sign of the input gradients scaled by ϵ , where the ϵ restricts ℓ_∞ of the perturbation. Kuerakin *et al.* [7] propose the Basic Iterative Method (BIM), which is an iterative version of FGSM and is also called Projected Gradient Descent (PGD). Madry *et al.* [5] show that PGD with randomly chosen starting points within allowed perturbation can make an attack stronger.

Defenses. The goal of the defense is to make a correct prediction on adversarial examples. However, adversarial defenses can cause obfuscated gradients which are easily broken by Backward Pass Differentiable Approximation attack [8]. Athalye *et al.* [8] recommend performing several sanity tests to check obfuscated gradients for a defense. Madry *et al.* [5] propose a defense based on the minimax formulation of adversarial training which has been extensively evaluated and justified. We also combine our method with the adversarial training and empirically show that our method does not rely on this fragile obfuscated gradients by following evaluations in [8]. However, the previous approach uses the conventional one-hot (*1ofK*) encoding for both source and target models, while we propose a higher dimensional multi-way encoding that obstructs the adversarial gradient search.

3 Our Approach

In this section we will explain our approach using the following notation: $g(x)$ is the target model to be attacked, and $f(x)$ is the substitute model used to generate a black-box attack for $g(x)$. In the case of a white-box attack, $f(x)$ is $g(x)$. Canonical attacks like FGSM and PGD are gradient-based methods. Such approaches perturb an input x by an amount dependent upon $\text{sign}(\nabla_x \text{Loss}(f(x)))$. An adversarial example x^{adv} is generated as follows:

$$x^{adv} = x + \epsilon \text{sign}(\nabla_x \text{Loss}(f(x))), \quad (1)$$

where ϵ is the strength of the attack. Therefore x^{adv} would be a translated version of x , in a vicinity further away from that of the ground-truth class, and thus becomes more likely to be misclassified, resulting in a successful adversarial attack. If the attack is a targeted one, x could be deliberately moved towards some other specific target class. This is conventionally accomplished by using the adversarial class as the ground truth when back-propagating the loss, and subtracting the perturbation from the original input. The assumption being made in such approaches is that their input gradient direction is similar: $\nabla_x \text{Loss}(f(x)) \approx \nabla_x \text{Loss}(g(x))$.

We now present the most widely used setup for training state-of-the-art deep classification networks comprising of one-hot encoding and softmax. Let the output activation of neuron i in the final encoding (fully-connected) layer be s_i , where $i = 1, 2, \dots, l$ and l is the encoding length. Then, the softmax probability y_i of s_i , the cross-entropy loss, and the partial derivative of the loss with respect to s_i are:

$$y_i = \frac{e^{s_i}}{\sum_{c=1}^k e^{s_c}}, \quad \text{Loss} = -\sum_{i=1}^k t_i \log(y_i), \quad \text{and} \quad \frac{\partial \text{Loss}}{\partial s_i} = y_i - t_i. \quad (2)$$

respectively, where k is the number of classes.

Combined with the most widely used one-hot (*1ofK*) encoding scheme, the derivative in Eqn. 2 makes the gradients of substitute and target models strongly correlated. We demonstrate this as follows: Given a ground-truth example belonging to class $[1, 0, \dots, 0]$, non-zero gradients of neuron 1 of the encoding layer will always be negative, while all other neurons will always be positive since $0 < y_i < 1$. So, regardless of the model architecture and the output, the signs of the partial derivatives are determined by the category, and thus the gradients for that category only lie in a limited hyperoctant (see Fig. 1 for the 2D case). This constraint causes strong correlation in gradients in the final layer for different models using the *1ofK* encoding. Our experiments suggest that this correlation can be carried all the way back to the input perturbations, making these models more vulnerable to attacks.

In this work, we aim to make $\nabla_x \text{Loss}(f(x))$ and $\nabla_x \text{Loss}(g(x))$ less correlated by encouraging *model decorrelation*. We do this by introducing multi-way encoding instead of the conventional *1ofK* encoding used by deep models for classification. Multi-way encoding significantly reduces the correlation between the gradients of the substitute and target models, making it more challenging for an adversary to create an attack that is able to fool the classification model.

The multi-way encoding we propose in this work is the Random Orthogonal (*RO*) output vector encoding generated via Gram-Schmidt orthogonalization. Starting with a random matrix $A = [a_1 | a_2 | \dots | a_n] \in \mathbb{R}^{k \times l}$, the first, second, and k^{th} orthogonal vectors are computed as follows:

$$\begin{aligned} u_1 &= a_1, & e_1 &= \frac{u_1}{\|u_1\|}, & u_2 &= a_2 - (a_2 \cdot e_1)e_1, & e_2 &= \frac{u_2}{\|u_2\|}, \\ u_k &= a_k - \dots - (a_k \cdot e_{k-1})e_{k-1}, & e_k &= \frac{u_k}{\|u_k\|}. \end{aligned} \quad (3)$$

For a classification problem of k classes, we create a codebook $C_{RO} \in \mathbb{R}^{k \times l}$, where $C^i = \beta e_i$ is a length l encoding for class i , and $i \in 1, \dots, k$, and β is a scaling hyper-parameter dependent upon l . A study on the selection of the length l is presented in the experiments section.

By breaking away from the *1ofK* encoding, softmax and cross-entropy become ill-suited for the model architecture and training. Instead, we use the loss between the output of the encoding-layer and the *RO* ground-truth vector, $\text{Loss}(f(x), t_{RO})$, where $f(x) \in \mathbb{R}^l$ and Loss measures the distance between $f(x)$ and t_{RO} . In our multi-way encoding setup, the final encoding (s) and $f(x)$ become

Table 1: This table presents the effect of increasing the dimension (10, 20, ..., 3000) of the output encoding layer of the multi-way encoding on the classification accuracy (%) for MNIST on FGSM black-box, white-box attacks ($\epsilon = 0.2$) and clean data. As the dimension increases, accuracy increases up to a certain point; We use 2000 for the length of our multi-way encoding layer.

	10	20	40	80	200	500	1000	2000	3000
Black-box	45.4	52.4	62.4	71.3	73.7	78.0	79.6	83.6	82.9
White-box	18.1	23.5	27.4	38.8	40.3	39.5	45.8	54.9	45.3
Clean	96.8	97.0	97.9	98.3	98.5	98.8	98.8	99.1	98.9

equivalent. Classification is performed using $\arg \min_i \text{Loss}(f(x), t_{RO}^i)$. We use Mean Squared Error (MSE) Loss.

Figure 1 illustrates how using a multi-way and longer encoding results in an increased number of possible gradient directions, reducing the probability of an adversary selecting a harmful direction that would cause misclassification. For simplicity we consider a binary classifier. Axis s_i in each graph represents the output activation of neuron i in the output encoding layer, where $i = 1, \dots, l$. The depicted points are correctly classified points for the green and blue classes. The arrows depict the sign of non-zero gradients $\frac{\partial \text{Loss}}{\partial s_i}$. (a) Using a $1ofK$ encoding and a softmax-cross entropy classifier, there are only two directions for a point to move, a direct consequence of $1ofK$ encoding together with Eqn. 2. Of these two directions, only one is an adversarial direction, depicted in red. (b) Using 2-dimensional multi-way encoding, we get four possible non-zero gradient directions. The fraction of directions that now move a correctly classified point to the adversarial class is reduced. (c) Using a higher dimension multi-way encoding results in a less constrained gradient space compared to that of $1ofK$ encoding. In the case of attacks formulated following Eqn. 1, this results in 2^l possible gradient directions, rather than l in the case of $1ofK$ encoding. The fraction of gradients whose direction would move an input from the green ground-truth class to the blue class, or vice versa, decreases significantly. In addition, multi-way encoding provides additional robustness by increasing the gradients’ dimensionality. The effect of increasing dimensionality is shown in Table 1.

We also combine multi-way encoding with adversarial training for added robustness. We use the following formulation to solve the canonical min-max problem [5, 9] against PGD attacks:

$$\arg \min_{\theta} [\mathbb{E}_{(x,y) \in p_{train}} \max_{\delta} (\mathcal{L}(\theta, x + \delta, y)) + \lambda \mathbb{E}_{(x,y) \in p_{train}} (\mathcal{L}(\theta, x, y))] \quad (4)$$

where p_{train} is the training data distribution, (x, y) are the training points, and λ determines a weight of the loss on clean data together with the adversarial examples at train time. For generating white-box adversarial attacks to our method, we minimize a variant of Carlini-Wagner (CW) loss [10]:

$$\max \left(\min_{i \neq t} \text{Loss}(x, e_i) - \text{Loss}(x, e_t), -\kappa \right) \quad (5)$$

where e_t is the ground-truth vector, κ is a confidence, and Loss is MSE loss.

4 Experiments

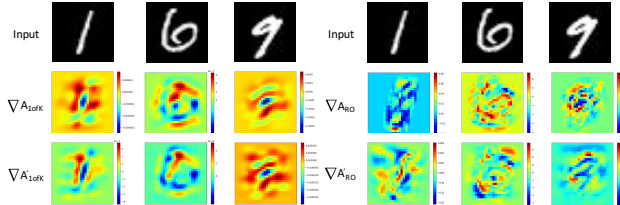
In this work we define a **black-box** attack as one where the adversary knows the architecture and the output encoding used but not learned weights. We use two substitute models using $1ofK$ and RO encodings respectively to evaluate our method. We define a **white-box** attack as one where the adversary knows full information about our model, including the learned weights. We conduct experiments on four commonly-used benchmark datasets: MNIST, CIFAR-10, CIFAR-100, and SVHN.

The threat model is a ℓ_{∞} bounded attack within the allowed perturbation ϵ : 0.3 MNIST, 8/255.0 CIFAR-10, 8/255.0 CIFAR-100, 10/255.0 SVHN by following [5, 11].

4.1 Multi-way Encoding on MNIST

In this section we provide an in-depth analysis of our multi-way encoding on the MNIST dataset. We conduct experiments to examine how multi-way output encodings can decorrelate gradients

Layer	Pearson Correlation Coefficient		
	A_{1ofK}, A'_{1ofK}	A_{RO}, A'_{RO}	A_{RO}, A_{1ofK}
Conv1	0.29	0.06	0.0
Conv2	0.24	0.15	0.01
Input	0.35	0.08	0.02



(a) Correlation of input gradients

(b) Visualization of input gradients

Figure 2: We present (a) three sample examples of input gradients from A_{1ofK} , A'_{1ofK} , A_{RO} , and A'_{RO} models. The gradients of $1ofK$ models become similar after training while the gradients of RO models are dissimilar. (b) the correlation coefficients of the gradients at each layer of the models. RO encoding results in a lower correlation of input gradients between models (model decorrelation).

(Sec. 4.1.1) and increase adversarial robustness (Sec. 4.1.2). We compare models trained on $1ofK$ output encodings with models having the same architecture but trained on multi-way output encodings. In all experiments we use RO encoding as the multi-way encoding with dimension 2000 determined by Table 1 and $\beta = 1000$. All models achieve $\sim 99\%$ on the clean test set. Models A and C are LeNet-like CNNs and inherit their names from [12]. We use their architecture with dropout before fully-connected layers. We trained models A and C on MNIST with the momentum optimizer and an initial learning rate of 0.01, $momentum = 0.5$ with different weight initializations. It should be noted that, in this section, substitute and target models are trained on clean data and do not undergo any form of adversarial training.

4.1.1 Model Decorrelation

In this section we present how multi-way encoding results in gradient decorrelation. For further comparison, we train models A'_{1ofK} and A'_{RO} , that are independently initialized from the models A_{1ofK} and A_{RO} . In Fig 2 (a) we present aggregate results on the entire MNIST dataset. We measure the correlation of gradients between all convolutional layers and the input layer of models trained on different encodings. We first compute the gradients of the loss with respect to intermediate features of Conv1 and Conv2. We average gradients of convolutional layers over channels in the same way a gradient-based saliency map is generated [13]. Otherwise, the order of convolutional filters affects the correlations and makes it difficult to measure proper correlations between models. Then, we compute the Pearson correlation coefficient (ρ) of the sign of the gradients with respect to the intermediate features between models. We find that the correlations of Conv1 and Conv2 between $1ofK$ models are much higher than those of RO models. It also shows that the correlations between RO and $1ofK$ are also low. In addition, RO models are not highly correlated even though they are using the same encoding scheme. At the input layer, the correlations between RO and $1ofK$ are almost zero, but $1ofK$ models have a significantly higher correlation.

In Fig 2 (b) we visualize the value of the gradients of the loss with respect to input (input gradients) from the models: A_{1ofK} , A'_{1ofK} , A_{RO} , and A'_{RO} , for three sample images from the MNIST dataset. We observe that the gradients of A_{1ofK} and A'_{1ofK} are more similar than those of A_{RO} and A'_{RO} . Also, the gradients of $1ofK$ encoding models are quite dissimilar compared to those of RO encoding models.

4.1.2 Robustness

Table 2 presents the classification accuracy (%) of target models under attack from various substitute models. Columns represent the substitute models used to generate FGSM attacks of strength $\epsilon = 0.2$ and rows represent the target models to be tested on the attacks. The diagonal represents white-box attacks and others represent black-box attacks. Every cell corresponds to an attack from a substitute model $f(x)$ for a target model $g(x)$. The last column reports the average accuracy on black-box attacks.

By comparing the last column of Table 2, the $g(x)$ using the $1ofK$ encoding is more vulnerable to black-box attacks than the corresponding $g(x)$ using the RO encoding. Black-box attacks become

Table 2: This table presents the classification accuracy (%) of MNIST on black-box and white-box FGSM attacks using architectures A and C. $f(x)$ is a substitute model and $g(x)$ is a target model. We conclude: (a) $g(x)$ using $1ofK$ is more vulnerable to black-box attacks than $g(x)$ using RO . (b) For white-box attacks, RO encoding leads to better accuracy compared to $1ofK$. (c) In brackets is the correlation coefficient of the input gradients of $g(x)$ and $f(x)$. RO results in a lower correlation compared to $1ofK$.

$f(x) \backslash g(x)$	A_{1ofK}	A_{RO}	C_{1ofK}	C_{RO}	AVG BB
A_{1ofK}	34.9 (1.00) *	93.6 (0.02)	56.8 (0.25)	95.5 (0.03)	82.0
A_{RO}	88.7 (0.02)	54.9 (1.00) *	92.5 (0.02)	82.9 (0.09)	88.0
C_{1ofK}	30.1 (0.25)	83.6 (0.01)	22.5 (1.00) *	93.3 (0.01)	69.0
C_{RO}	94.3 (0.03)	87.5 (0.09)	96.1 (0.01)	70.5 (1.00) *	92.6

stronger if $f(x)$ uses the same encoding as $g(x)$. In addition, even though the same encoding is used, RO models maintain higher robustness to the black-box attacks compared to $1ofK$ models (e.g. 82.9% when C_{RO} attacks A_{RO} vs. 56.8% when C_{1ofK} attacks A_{1ofK}). This suggests that RO encoding is more resilient to black-box attacks.

It is also evident from the results of this experiment in Table 2 that even when the source and target models are the same, denoted by (*), RO encoding leads to better accuracy, and therefore robustness to white-box attacks, compared to $1ofK$ encoding.

Finally, Table 2 also reports the correlation coefficient of $sign(\nabla_x Loss(f(x)))$ and $sign(\nabla_x Loss(g(x)))$ in Eqn. 1. These gradients are significantly less correlated when the source and target models use different encodings. In addition, RO results in a lower correlation compared to $1ofK$ when the same encoding is used in the source and target models.

We present ablation studies on our method in Section B in Appendix.

4.2 Benchmark Results

In this section we analyze the case where we combine our method with adversarial training (Eq 4). We compare against the strong baseline of Madry *et al.* [5], which also uses adversarial training. For adversarial training, we use a mix of clean and adversarial examples for MNIST, CIFAR-10, and CIFAR-100, and adversarial examples only for SVHN following the experimental setup and the threat models used by Madry *et al.* [5] and Buckman *et al.* [11]. We use PGD attacks with a random start, and follow the PGD parameter configuration of [5, 9, 11].

We directly compare our method with the publicly released versions of Madry *et al.* [5] on MNIST and CIFAR-10 in Table 3. We present results for 1K-step PGD black-box attacks generated from the independently trained copy of Madry *et al.* (the first column) and the model trained with the RO (the second column). It should be noted that the substitute model uses the same RO encoding parameters used for the target model. We generate 1K-step PGD white-box attacks with a random start. In addition, we generate 5K-step PGD attacks with 50 random restarts.

Table 3 demonstrates the robustness of multi-way encoding for black-box attacks, while at the same time maintaining a high accuracy for white-box attacks and clean data.

The black-box attacks of the second column show the robustness even when an adversary knows the exact value of the encoding used for the target model. We generate high-confidence PGD attacks with Eq. 5 from the independently trained copy of the RO model. Our model still achieves higher robustness compared to the baseline. In CIFAR-10, the black-box attacks from the RO model (*i.e.* the substitute model uses the same RO encoding parameters) are much weaker than the black-box attacks from the $1ofK$ model. This shows that RO can effectively decorrelate the target model even when the encoding is exposed to an adversary. This is also consistent with the results in Fig. 2 (a) where the correlation of gradients are lower and higher the black-box robustness of the RO models in Table 2 even when the substitute model uses the same RO encoding as the target model. In the third and fourth columns, our defense also achieves higher robustness than the baseline on PGD white-box attacks.

Table 3: Comparison against the released models of Madry *et al.* [5] on white-box, black-box PGD attacks, gradient-free attacks and on clean data. We report results on white and black-box PGD attacks generated using the 1K iterations. We observe that our approach is more resilient to these types of attacks and obtains improvements on clean data.

Dataset	Model	Accuracy (%)					
		Blackbox #steps:1K (1ofK)	Blackbox #steps:1K (RO)	Whitebox #steps:1K	Whitebox #steps:5K 50-restarts	Gradient -free	Clean
MNIST	Madry <i>et al.</i> [5]	94.9	95.0	92.2	89.6	35.4	98.4
	Ours	96.9	96.8	94.9	94.1	42.7	99.2
CIFAR-10	Madry <i>et al.</i> [5]	62.5	73.8	45.3	44.9	46.6	87.3
	Ours	65.2	72.2	53.1	52.4	56.9	89.4

Table 4: Evaluation on common corruptions and perturbations on CIFAR-10 [14]. Our method obtains higher accuracy (test accuracy %) in all cases. (See Table 9 in Appendix for all perturbations.)

Model	Corruptions								
	All	Bright.	Spatter	Jpeg	Elestic	Motion	Zoom	Impulse	Speckle
Madry <i>et al.</i>	81.5	87.1	81.6	85.4	81.7	80.4	82.7	68.8	81.8
Ours	83.4	89.3	84.4	87.1	83.2	81.6	84.0	72.0	84.3

We follow [15, 16] and perform gradient-free attacks to check for signs of obfuscated gradients. In the fifth column, we evaluate our method on gradient-free attacks; (1) decision-based attacks [17, 18] for MNIST and (2) query-based attacks [19] using Eq. 5 for CIFAR-10. It should be noted the decision-based attacks are ℓ_2 bounded which violates our threat model. From the results, gradient-free attacks could not break our defense and we do not observe a sign of obfuscated gradients.

Ford *et al.* [20] highlight the close relationship between adversarial robustness and general corruption (*e.g.* Gaussian noise) robustness. They argue that a defense should have higher robustness on general corruptions and recommend reporting corruption robustness as a sanity check for a defense. Therefore, we evaluate our method’s general robustness, using the dataset of Hendrycks *et al.* [14] that is designed to test the common corruptions and perturbations on CIFAR-10. As reported in Table 4, we achieve higher robustness in all cases.

4.3 Further Evaluations

We train the method of Madry *et al.* and our approach on CIFAR-100 and SVHN. Fig. 3 represents the robustness on black-box and white-box attacks on different PGD attack iterations. We also report the clean accuracy when the iteration = 0.

Our method achieves higher robustness on the black-box and white-box attacks on CIFAR-100 and SVHN. In addition, we also improve the clean accuracy by 7% on CIFAR-100.

In order to further evaluate our defense, we provide evaluations by following the guidelines of Athalye *et al.* [8] to check if our method relies on obfuscated gradients. We include plots of intermediate PGD attack iterations in Fig. 3. Transfer-based attacks can effectively check if a defense method relies on obfuscated gradients [8]. Our model is robust to the transfer-based attacks from Madry *et al.*. In addition, we observe that (1) the attack is converged; (2) iterative attacks are stronger than single-step attacks; (3) white-box attacks are stronger than black-box attacks. From the evaluations above, we do not find a sign of obfuscated gradients and our defense performs better than the baseline.

We present further analysis on white-box attacks in Sections C and D of Appendix.

5 Application: Attacking Model Watermarking

Zhang *et al.* [6] introduced an algorithm to detect whether a model is stolen or not. They do so by adding a watermark to sample images of specific classes and deliberately training the model to misclassify these examples to other specific classes. Even if their pre-trained model is stolen, the

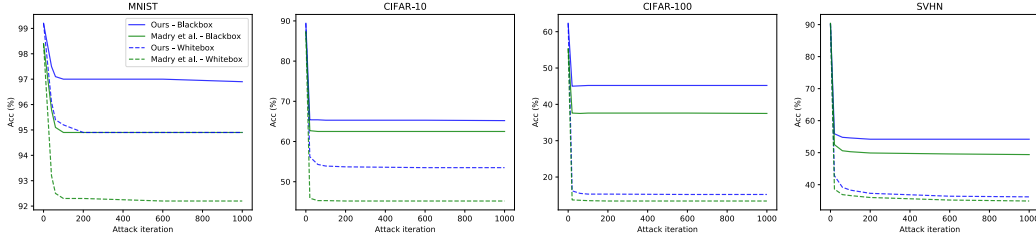


Figure 3: We generate PGD attacks with different number of iterations and compare our method with the baseline by following [8]. Black-box attacks are generated from an independently trained copy of the baseline. We observe that (1) the attack is converged; (2) iterative attacks are stronger than single-step attacks; (3) white-box attacks are stronger than black-box attacks.

	Finetune?	Test Acc (%)	Watermarking Acc (%)
StolenNet _{1ofK}	✗	84.7	98.6
Net _{1ofK}	✗	48.3	6.1
Net _{RO}	✗	48.0	10.0
Net _{1ofK}	✓	85.6	87.8
Net _{RO}	✓	80.2	12.9

Table 5: We present that RO encoding can fool the watermarking detection by model decorrelation. Fine-tuning using RO encoding remarkably reduces transferability of watermarked images (*i.e.* watermarking acc) while taking advantage of the pre-trained weights of the stolen model.

model should make a misclassification on the watermarked image. This work has demonstrated to be robust even when the model is fine-tuned on a different training set.

We interpret the watermarked image used to deliberately cause a misclassification as a *transferable adversarial example*. We introduce an attack for this algorithm using our multi-way encoding, making it more challenging to detect whether a model is stolen or not. We do this by fine-tuning the stolen model using multi-way encoding, rather than the encoding used in pre-training the model. We show that our multi-way encoding successfully decorrelate a model from the pre-trained model and, as a result, adversarial examples become less transferable.

We follow the same CIFAR-10 experimental setup for detecting a stolen model as in Zhang *et al.*: We split the test set into two halves. The first half is used to fine-tune pre-trained networks, and the second half is used to evaluate new models. When we fine-tune the *1ofK* model, we re-initialize the last layer. When we fine-tune the *RO* model we replace the output encoding layer with our 2000-dimension fully-connected layer, drop the softmax, and freeze convolutional weights.

We present results on the CIFAR-10 dataset in Table 5. When the fine-tuning was performed using the *1ofK* encoding (also used in pre-training the model), watermarking detection is 87.8%, and when the fine-tuning was performed using the multi-way *RO* encoding the watermarking detection is only 12.9% while taking advantage of the pre-trained weights of the stolen model. The watermark detection rate of the model fine-tuned using *RO* is significantly lower than that fine-tuned using *1ofK* encoding, and is more comparable to models that are trained from scratch and do not use the stolen model (6.1% and 10.0%). This results suggest that our multi-way encoding successfully decorrelate the target model (finetuned **Net**_{RO}) from the source model (**Stolen Net**_{1ofK}).

6 Conclusion

By relaxing the *1ofK* encoding to a real number encoding, together with increasing the encoding dimensionality, our multi-way encoding decorrelates source and target models, confounding an attacker by making it more difficult to perturb an input in gradient direction(s) that would result in misclassification of a correctly classified example. We present stronger robustness on four benchmark datasets for both black-box and white-box attacks and we improve classification accuracy on clean data. We also demonstrate the strength of our approach by introducing an attack for model watermarking, decorrelating a target model from the source model.

Acknowledgments

We thank Kate Saenko, Vitaly Ablavsky, Adrian Vladu, Seong Joon Oh, Tae-Hyun Oh, and Bryan Plummer for helpful discussions. This work was supported in part by gifts from Adobe.

References

- [1] Christian Szegedy, Wojciech Zaremba, Ilya Sutskever, Joan Bruna, Dumitru Erhan, Ian Goodfellow, and Rob Fergus. Intriguing properties of neural networks. *arXiv preprint arXiv:1312.6199*, 2013.
- [2] Nicolas Papernot, Patrick McDaniel, and Ian Goodfellow. Transferability in machine learning: from phenomena to black-box attacks using adversarial samples. *arXiv preprint arXiv:1605.07277*, 2016.
- [3] Yanpei Liu, Xinyun Chen, Chang Liu, and Dawn Song. Delving into transferable adversarial examples and black-box attacks. *arXiv preprint arXiv:1611.02770*, 2016.
- [4] Ian J Goodfellow, Jonathon Shlens, and Christian Szegedy. Explaining and harnessing adversarial examples. *arXiv preprint arXiv:1412.6572*, 2014.
- [5] Aleksander Madry, Aleksandar Makelov, Ludwig Schmidt, Dimitris Tsipras, and Adrian Vladu. Towards deep learning models resistant to adversarial attacks. *arXiv preprint arXiv:1706.06083*, 2017.
- [6] Jialong Zhang, Zhongshu Gu, Jiyong Jang, Hui Wu, Marc Ph Stoecklin, Heqing Huang, and Ian Molloy. Protecting intellectual property of deep neural networks with watermarking. In *Proceedings of the 2018 on Asia Conference on Computer and Communications Security*, pages 159–172. ACM, 2018.
- [7] Alexey Kurakin, Ian Goodfellow, and Samy Bengio. Adversarial examples in the physical world. *arXiv preprint arXiv:1607.02533*, 2016.
- [8] Anish Athalye, Nicholas Carlini, and David Wagner. Obfuscated gradients give a false sense of security: Circumventing defenses to adversarial examples. *arXiv preprint arXiv:1802.00420*, 2018.
- [9] Harini Kannan, Alexey Kurakin, and Ian Goodfellow. Adversarial logit pairing. *arXiv preprint arXiv:1803.06373*, 2018.
- [10] Nicholas Carlini and David Wagner. Towards evaluating the robustness of neural networks. *arXiv preprint arXiv:1608.04644*, 2016.
- [11] Jacob Buckman, Aurko Roy, Colin Raffel, and Ian Goodfellow. Thermometer encoding: One hot way to resist adversarial examples. 2018.
- [12] Florian Tramèr, Alexey Kurakin, Nicolas Papernot, Ian Goodfellow, Dan Boneh, and Patrick McDaniel. Ensemble adversarial training: Attacks and defenses. *arXiv preprint arXiv:1705.07204*, 2017.
- [13] Ramprasaath R Selvaraju, Michael Cogswell, Abhishek Das, Ramakrishna Vedantam, Devi Parikh, Dhruv Batra, et al. Grad-cam: Visual explanations from deep networks via gradient-based localization. In *ICCV*, pages 618–626, 2017.
- [14] Dan Hendrycks and Thomas Dietterich. Benchmarking neural network robustness to common corruptions and perturbations. *arXiv preprint arXiv:1903.12261*, 2019.
- [15] Nicholas Carlini, Anish Athalye, Nicolas Papernot, Wieland Brendel, Jonas Rauber, Dimitris Tsipras, Ian Goodfellow, and Aleksander Madry. On evaluating adversarial robustness. *arXiv preprint arXiv:1902.06705*, 2019.
- [16] Jonathan Uesato, Brendan O’Donoghue, Aaron van den Oord, and Pushmeet Kohli. Adversarial risk and the dangers of evaluating against weak attacks. *arXiv preprint arXiv:1802.05666*, 2018.

- [17] Wieland Brendel, Jonas Rauber, and Matthias Bethge. Decision-based adversarial attacks: Reliable attacks against black-box machine learning models. *arXiv preprint arXiv:1712.04248*, 2017.
- [18] Lukas Schott, Jonas Rauber, Matthias Bethge, and Wieland Brendel. Towards the first adversarially robust neural network model on mnist. 2018.
- [19] Yandong Li, Lijun Li, Liqiang Wang, Tong Zhang, and Boqing Gong. NATTACK: A STRONG AND UNIVERSAL GAUSSIAN BLACK-BOX ADVERSARIAL ATTACK, 2019.
- [20] Nic Ford, Justin Gilmer, Nicolas Carlini, and Dogus Cubuk. Adversarial examples are a natural consequence of test error in noise. *arXiv preprint arXiv:1901.10513*, 2019.
- [21] Yann LeCun, Léon Bottou, Yoshua Bengio, and Patrick Haffner. Gradient-based learning applied to document recognition. *Proceedings of the IEEE*, 86(11):2278–2324, 1998.
- [22] Alex Krizhevsky and Geoffrey Hinton. Learning multiple layers of features from tiny images. Technical report, Citeseer, 2009.
- [23] Yuval Netzer, Tao Wang, Adam Coates, Alessandro Bissacco, Bo Wu, and Andrew Y Ng. Reading digits in natural images with unsupervised feature learning. In *NIPS workshop on deep learning and unsupervised feature learning*, volume 2011, page 5, 2011.
- [24] Kaiming He, Xiangyu Zhang, Shaoqing Ren, and Jian Sun. Deep residual learning for image recognition. In *Proceedings of the IEEE conference on computer vision and pattern recognition*, pages 770–778, 2016.
- [25] Sergey Zagoruyko and Nikos Komodakis. Wide residual networks. *arXiv preprint arXiv:1605.07146*, 2016.
- [26] Logan Engstrom, Andrew Ilyas, and Anish Athalye. Evaluating and understanding the robustness of adversarial logit pairing. *arXiv preprint arXiv:1807.10272*, 2018.
- [27] Nicholas Carlini and David Wagner. Defensive distillation is not robust to adversarial examples. *arXiv preprint arXiv:1607.04311*, 2016.
- [28] Shuo Yang, Ping Luo, Chen Change Loy, Kenneth W Shum, Xiaoou Tang, et al. Deep representation learning with target coding. In *AAAI*, pages 3848–3854, 2015.
- [29] Pau Rodríguez, Miguel A Bautista, Jordi González, and Sergio Escalera. Beyond one-hot encoding: Lower dimensional target embedding. *Image and Vision Computing*, 75:21–31, 2018.

Appendix

A Experimental Details

A.1 Dataset

MNIST [21] is a dataset of handwritten digits. It has a training set of 60K examples, and a test set of 10K examples. For MNIST, Madry *et al.* use 90% of the training set for training. We follow the same training setup. **CIFAR-10** [22] is a canonical benchmark for image classification and retrieval, with 60K images from 10 classes. The training set consists of 50K images, and the test set consists of 10K images. **CIFAR-100** [22] is similar to CIFAR-10 in format, but has 100 classes containing 600 images each. Each class has 500 training images and 100 testing images. **SVHN** [23] is an image dataset for recognizing street view house numbers obtained from Google Street View images. The training set consists of 73K images, and the test set consists of 26K images.

A.2 Model Architecture

For MNIST and CIFAR-10, we follow the experimental settings in Madry *et al.* [5]; for MNIST we use LeNet, for CIFAR-10 we use a ResNet [24] of Madry *et al.*. For CIFAR-100 and SVHN we use a WideResNet [25] of depth 28 and 16, respectively, with a width factor 4 and a dropout of 0.3 following [11]. We use the optimizer used by [5, 11].

B Ablation Study on Encodings

We perform ablation studies to further investigate the effectiveness of our *RO* encoding. We train the model used in Table 2 in the original manuscript with two different combinations of encodings and loss functions. Please note that the two alternative models have 10 dimensions at the last layer while *RO* has 2000 dimensions.

B.1 Alternative approach

B.1.1 $RO_{softmax}$

We evaluate a network that uses *RO* encoding, a softmax layer, and cross-entropy loss. We compute the probability of i^{th} class as follows:

$$P(i|s) = \frac{\exp(\mathbf{s}^\top \mathbf{e}_i)}{\sum_{j=1}^n \exp(\mathbf{s}^\top \mathbf{e}_j)}$$

where \mathbf{s} is the ℓ_2 normalized final layer representation, \mathbf{e}_i is the *RO* encoding vector (ground-truth vector) from the codebook, and n is the number of classes.

B.1.2 $1ofK_{MSE}$

We also evaluate a network that uses mean-squared error (MSE) loss with the $1ofK$ encoding.

B.2 Evaluation

We generate FGSM attacks with $\epsilon = 0.2$ from substitute models A_{1ofK} and C_{1ofK} on MNIST to evaluate the models of Section B.1.1 and Section B.1.2. We also measure a correlation coefficient of the sign of the input gradients between target and substitute models as explained in Section 4.1.1. Tables 6 and 7 demonstrate that *RO*, among the different target models, achieves the highest accuracy and the lowest input gradient correlation with the substitute model. It should be noted that the two alternative models have 10 neurons at the last layer while *RO* has 2000 neurons. In addition, $RO_{softmax}$ has a softmax layer so that the gradients at the final layer are determined by a ground-truth class of an example.

Table 6: This table presents black-box attacks from the substitute model A_{1ofK} on various target models. RO achieves the highest accuracy and the lowest input gradient correlation with the substitute model among the different target models.

Target Model	A			C		
	$RO_{softmax}$	$1ofK_{MSE}$	RO	$RO_{softmax}$	$1ofK_{MSE}$	RO
Accuracy (%)	48.7	43.4	88.7	53.7	42.1	94.3
Correlation Coefficient	0.14	0.15	0.02	0.1	0.13	0.03

Table 7: This table presents black-box attacks from the substitute model C_{1ofK} on various target models. RO achieves the highest accuracy and the lowest input gradient correlation with the substitute model among the different target models.

Target Model	A			C		
	$RO_{softmax}$	$1ofK_{MSE}$	RO	$RO_{softmax}$	$1ofK_{MSE}$	RO
Accuracy (%)	67.4	55.9	92.5	62.6	58.8	96.1
Correlation Coefficient	0.08	0.09	0.02	0.08	0.1	0.01

C Checking for Signs of Obfuscated Gradients

In order to check if our method relies on obfuscated gradients [8], we report the accuracies on white-box attacks by varying epsilon on CIFAR-10 in Table 8. Maximum allowed perturbation for our model is $8/255$, but we use larger epsilon to check the behavior of our model. We checked that increasing distortion bound monotonically increase attack success rates and unbounded attacks achieve 100% attack success rate.

Table 8: This table presents accuracies on white-box attacks by varying epsilon (ℓ_∞).

epsilon	2	4	6	10	12	14	18	20	Unbounded
Accuracy (%)	78.9	66.7	55.8	53.0	50.4	48.1	29.7	27	0

D Analysis on White-box Attacks

The goal of this section is to understand how our method improves white-box robustness in order to further analyze our model. Following [26], we plot the landscapes of the loss of our method and the value of neurons that correspond to ground-truth class of the baseline model [5] for CIFAR-10. Since cross-entropy loss with a softmax layer can be biased to the norm of neuron values at the final layer (Section 3 in [27]), we instead plot the value of the ground-truth neuron for the baseline model. In Fig. 4, The x-axis represents the magnitude of the direction of $r_1 = \text{sign}(\nabla_{x'} \text{Loss}(f(x')))$ and the y-axis represents the magnitude of a random direction, $r_2 \sim \text{Rademacher}(0.5)$. For our model, z-axis represents the mean squared error loss between the final encoding and the ground-truth vector at each input data point ($x^{adv} = x' + x * r_1 + y * r_2$). For Madry *et al.*, the z-axis represents the value of the ground-truth neuron in the final layer which is directly responsible for the loss.

For Madry *et al.*, the landscapes show linearity along with the direction of r_1 for over the test set regardless of misclassification. However, our model shows non-linear behaviors over correctly classified examples but linear-like behaviors for misclassified examples. We show representative landscapes from the three test points. Fig. 4 (a) shows the linearity along with the direction of r_1 for the baseline. The value of #4 decreases slowly but still shows linear behavior and the values of #2 and #9 decrease significantly. 4 argue that the linearity is a primary cause of vulnerability. We also claim that the linear behavior makes it easier to find useful gradients. Fig. 4 (b), we observe that our

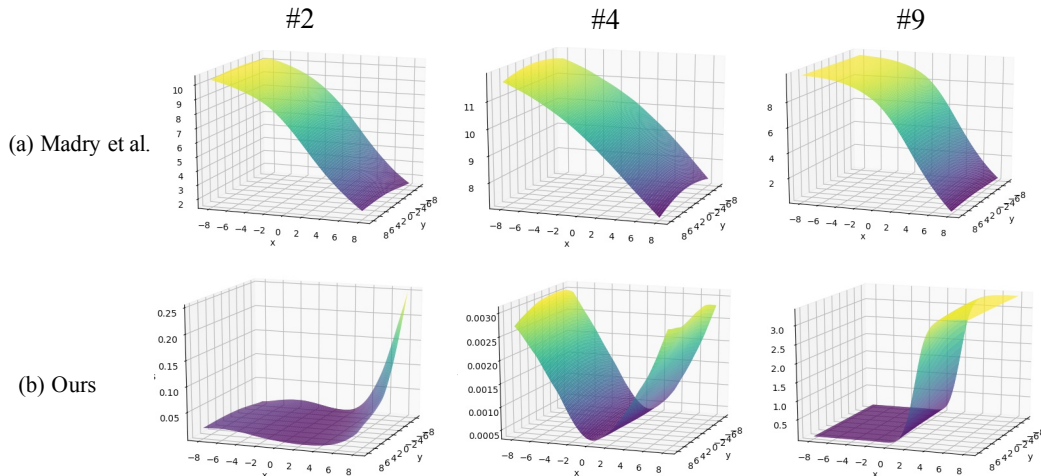


Figure 4: Comparisons of landscapes of the baseline model of Madry *et al.* [5] and our model. The x-axis represents the magnitude of the gradient direction of the loss w.r.t. input, the y-axis represents the magnitude of a random direction, and the z-axis represents (a) the value of the ground-truth neuron in the final layer for the baseline, and (b) the mean squared error loss between the final encoding and the ground-truth vector at each input data point ($x^{adv} = x' + x * r_1 + y * r_2$). In this figure, we depict the landscapes of x' being the second, fourth, and ninth test examples in the CIFAR-10 dataset.

model shows non-linear behavior with the direction of r_1 for the correctly classified examples: #2, #4. For #9, the more linear-like behavior results in a much higher loss and misclassification.

When ground-truth vectors are one-hot encodings, decreasing the output value of the neuron corresponding to the ground-truth class significantly would cause a misclassification. However, when ground-truth vectors are multi-way encodings, no single neuron is solely responsible for misclassification, but a more complex combination of neurons. Since the loss in our model is computed on multiple neurons at the final layer, an adversarial direction may increase the loss of certain neurons but it may also decrease the loss of other neurons at the same time. We argue that non-linearity is related to our high dimensional encoding layer which provides additional robustness to white-box attacks in addition to black-box attacks.

E Evaluation on common corruptions and perturbations on CIFAR-10

Table 9 reports all results on common corruptions and perturbations of CIFAR-10 [14].

F Transferability

In Table 3 of the main paper, the black-box attacks of the second column reports the robustness on black-box attacks from the independently trained copy of the *RO* model. In this section, we analyze the black-box attack accuracy on CIFAR-10 by varying confidence κ of Eq. 5 in the main paper. The higher confidence makes an attack to be more confident misclassification. We observe that the black-box attack accuracy converges at confidence= 1500. We report the lowest accuracy in Table 3.

G Related Work

Output encoding. There have been attempts to use alternate output encodings, also known as target encodings, for image classification in deep models. For example, Yang *et al.* [28] and Rodriguez *et al.* [29] use an output encoding that is based on Error-Correcting Output Codes (ECOC), for increased performance and faster convergence, but not for adversarial defense. In contrast, we use an alternate output encoding scheme, multi-way encoding, to make models more robust to adversarial attacks

Table 9: This table presents the all results on common corruptions and perturbations on CIFAR-10 [14]. Our method obtains higher test accuracy (%) in all cases.

Model	Corruptions			
	Brightness	Spatter	Jpeg	Elastic
Madry	87.1	81.7	85.4	81.7
Ours	89.3	84.4	87.1	83.2
	Motion	Zoom	Impulse	Speckle
Madry	80.4	82.7	68.8	81.8
Ours	81.6	84.0	72.0	84.3
	Saturate	Frost	Gauss. noise	Shot
Madry	84.3	85.5	82.2	82.8
Ours	86.3	87.8	84.3	85.1
Model	Glass	Fog	Gauss. blur	Pixelate
Madry	80.2	72.6	82.1	85.3
Ours	81.0	75.9	83.1	87.4
	Contrast	Defocus	Snow	AVG
Madry	77.0	83.6	82.6	81.5
Ours	78.9	85.0	84.7	83.4

Table 10: This table presents accuracies on black-box attacks from RO by varying confidence (κ). We generate 1000-step PGD attacks on CIFAR-10.

confidence	10	300	1500	3000	6000
Accuracy (%)	83.0	80.9	72.2	72.2	72.2